

# Analysis of Series-Connected Discrete Josephson Transmission Line

Hamid Reza Mohebbi, *Student Member, IEEE*, and A. Hamed Majedi, *Member, IEEE*

**Abstract**—Employing a generalized resistive–capacitive shunted junction model for Josephson junctions (JJs), the nonlinear wave propagation in the series-connected discrete Josephson transmission line (DJTL) is investigated. A DJTL consists of a finite number of unit cells, each including a segment of superconducting transmission line with a single array stack, or generally a block including an  $N$  identical lumped JJ element. As the governing nonlinear wave propagation is a system of nonlinear partial differential equations with mixed boundary conditions, the method of the finite difference time domain is used to solve the equations. By this numerical technique, the behavior of wave propagation along the DJTL can be monitored in time and space domains. Cutoff propagation, dispersive behavior, and shock-wave formation through the DJTL is addressed in this paper.

**Index Terms**—Dispersion equation, finite-difference time-domain (FDTD) method, Josephson junction (JJ) devices, microwave superconductivity, nonlinear inductance, nonlinear transmission lines (TLs), nonlinear wave propagation, shock waves.

## I. INTRODUCTION

**S**IGNIFICANT improvements on the performance of a wide variety of passive microwave devices and systems can be achieved by using superconducting materials due to their ultra-low surface resistance, frequency-independent penetration depth, and kinetic inductance. Ultra-low loss, high quality factor, and ultra-low dispersive behavior in superconducting microwave devices, such as transmission lines (TLs), cavity resonators, bandpass filters, and delay lines are the main consequences of these properties. Superconducting microwave devices have found niche applications in satellite and mobile communication systems, high-quality signal processing systems, RADAR [1]–[3], and more recently in circuit cavity quantum electrodynamics and quantum information processors [4], [5].

Greater flexibility in the design of superconductive passive and active microwave devices can be obtained by using Josephson junctions (JJs). Two basic electrical properties of JJs, useful for microwave devices, are nonlinear current-dependent inductive behavior and the ability to produce a high-frequency

signal from a dc-bias voltage. Since the inductance associated with each JJ is quite small, an array or stack of JJs can be effectively used to achieve any desired amount of inductance [6], [7]. Incorporation of an unbiased array of JJs in a typical superconducting TL will produce an ultra-low-loss nonlinear TL. Propagation characteristics of such nonlinear TLs are highly dependent on the collective behavior of the JJs that are in either series connection or parallel connection geometries across the TL. These structures are called either series- or parallel-connected discrete Josephson transmission line (DJTL). Although the parallel-connected DJTL has already been investigated in the past [7], more emphasis was placed on the study of nonlinear fluxon dynamics for rapid single flux quantum (RSFQ) applications rather than microwave device applications [8]. Moreover, the analysis of such a structure was previously performed based on circuit analysis [7], [9] or frequency-domain techniques [10]. In this paper, we use a nonlinear finite-difference time-domain (FDTD) technique to solve TL equations in order to monitor transient and steady-state response of the series-connected DJTL.

We aim to develop a systematic study of JJ-based microwave/millimeter-wave and terahertz devices, to take advantage of their unique properties for making planar superconductive parametric devices and integrated active/passive superconducting microwave/millimeter-wave/terahertz circuits for applications in superconducting opto-electronics [11] and quantum information processing [12] where high sensitivity and ultra-low-noise operation are on demand.

In this paper, we focus on the analysis of propagation characteristics and features of the series-connected DJTL as the simplest and the most natural way to incorporate JJs in a typical superconducting TL, e.g., microstrip line. In Sections II, the circuit model of the JJ and the equivalent nonlinear inductor are briefly described. In Section III, the physical implementation and mathematical analysis of a series-connected DJTL is presented. Details of the new nonlinear FDTD method to analyze the nonlinear microwave propagation are discussed in Section IV. Section V reports our simulation results based on the FDTD technique. With this new approach, we observe all the features associated with a typical nonlinear TL. They include cutoff propagation, controllable dispersive behavior, and shock-wave formation.

## II. CIRCUIT MODEL FOR LUMPED JJ

A JJ is a weak link between two superconductor electrodes. The weak link can be provided by several ways such as a thin-film insulator, microbridge, or point contact [13]. In the basic JJ, the current that can be driven through the junction is

Manuscript received October 31, 2008; revised April 18, 2009. First published July 07, 2009; current version published August 12, 2009. This work was supported in part under an Ontario Graduate Scholarship (OGS), by Quantum Works, and by the Institute for Quantum Computing (IQC), University of Waterloo.

The authors are with the Department of Electrical and Computer Engineering and the Institute for Quantum Computing (IQC), University of Waterloo, Waterloo, ON, Canada N2L 3G1 (e-mail: hmohebbi@maxwell.uwaterloo.ca; ahmajedi@maxwell.uwaterloo.ca).

Color versions of one or more of the figures in this paper are available online at <http://ieeexplore.ieee.org>.

Digital Object Identifier 10.1109/TMTT.2009.2025413

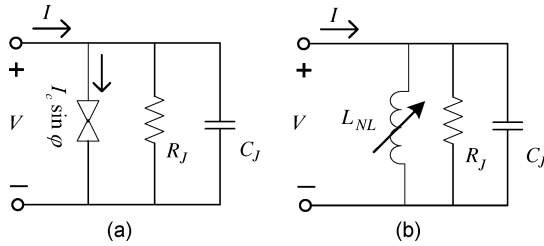


Fig. 1. (a) Generalized RCSJ model of JJ. The element denoted by the cross sign in this model is referred as a basic JJ element. (b) Basic JJ is replaced by a nonlinear inductance.

restricted to be less than the critical value, which is denoted by  $I_c$ . Two canonical relations that describe the circuit model of a basic JJ are

$$I(t) = I_c \sin \varphi(t) \quad (1)$$

$$V(t) = \frac{\Phi_0}{2\pi} \frac{d\varphi(t)}{dt} \quad (2)$$

where  $\Phi_0$  is a magnetic flux quanta with a value of  $\Phi_0 = 2.0679 \times 10^{-15} \text{ T} \cdot \text{m}^2$ , and  $I_c$  is the critical current of the JJ. By eliminating the phase difference between two superconductors, a basic JJ can be replaced by a nonlinear inductance [6], as shown in Fig. (1b). This nonlinear inductor satisfies the following equations:

$$V = L_J \frac{dI}{dt} \quad (3)$$

$$L_J = \frac{L_{J0}}{\sqrt{1 - \left(\frac{I}{I_c}\right)^2}} \quad (4)$$

where

$$L_{J0} = \frac{\Phi_0}{2\pi I_c} = \frac{\hbar}{2eI_c}. \quad (5)$$

The advantage of describing the Cooper pairs flow by a nonlinear inductive channel over the conventional relation  $I = I_c \sin \varphi$  is the fact that we can only deal with voltage and current rather than phase difference. The complete electrical characteristics of the generalized JJ are captured by the resistive–capacitive shunted junction (RCSJ) circuit model, as illustrated in Fig. (1a). The equations describing the behavior of the generalized JJ are [14]

$$V(t) = \frac{\Phi_0}{2\pi} \frac{d\varphi}{dt} \quad (6)$$

$$I(t) = I_c \sin \varphi + \frac{1}{R_J} \frac{\Phi_0}{2\pi} \frac{d\varphi}{dt} + C_J \frac{\Phi_0}{2\pi} \frac{d^2\varphi}{dt^2}. \quad (7)$$

Josephson critical current  $I_c$  is a figure of merit for the junction, which depends on the quality of superconductors and the geometry of the junctions. According to (4), nonlinearity plays a significant role when the driving current is very close to the critical current; as a result, the effect of nonlinearity becomes stronger when the critical current of the junction is small (typically less than  $10 \mu\text{A}$ ). Replacing the basic JJ element with a nonlinear inductor, a Josephson tunnel junction can be viewed as

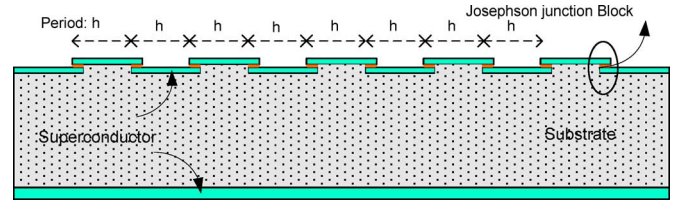


Fig. 2. Series-connected DJTL on a microstrip line (S–I–S junctions).

a nonlinear oscillator in a lossy medium, as depicted in Fig. (1b), which oscillates at the plasma frequency

$$\omega_p = \frac{1}{\sqrt{L_{J0} C_J}} = \left( \frac{2\pi I_c}{\Phi_0 C_J} \right)^{1/2}. \quad (8)$$

The characteristic “quality factor” of the oscillator is

$$Q = \sqrt{\beta_c} = \omega_p R_J C_J \quad (9)$$

where  $\beta_c$  is called the Stewart–McCumber parameter describing the shape of the dc  $I$ – $V$  characteristics of the junction. Plasma frequency of the junction determines the characteristic time scale of the dynamical process in the junction.

For a  $3 \mu\text{m} \times 3 \mu\text{m}$  JJ constructed by Nb– $\text{AlO}_x$ –Nb technology offered by HYPRESS in a high current density process, the junction’s parameters are  $I_c = 405 \mu\text{A}$ ,  $T_c = 9.2 \text{ K}$ ,  $T = 4.2 \text{ K}$ ,  $C_J = 0.531 \text{ pF}$ , and  $R_J = 3.2 \Omega$  [15], [16], which yields  $L_{J0} = 0.812 \text{ pH}$ ,  $\omega_p = 1.522 \text{ Trad/s}$ , and  $\beta_c = 6.73$ . Considering another junction made of Pb–PbO–Pb, the measured junction’s parameters are  $I_c = 254 \mu\text{A}$ ,  $T_c = 7.19 \text{ K}$ ,  $T = 4.2 \text{ K}$ ,  $C_J = 5 \text{ fF}$ , and  $R_J = 20 \Omega$ , thus  $L_{J0} = 1.2 \text{ pH}$ , which is so small [13], [17]. Therefore, arrays or stacks of  $N$  JJs are used to increase the total inductance of the structure. This array can be represented by a single junction with  $N$  times larger inductance,  $N$  times larger resistance, and  $N$  times smaller capacitance compared to a single junction, upon the condition of identical junctions, because there exists three distinct channels for current flow in a typical JJ: inductive channel for cooper pairs, resistive channel for normal electron, and capacitive channel for displacement current. The total inductive channels, Cooper pair’s flow, can be delineated by the total phase difference  $\varphi$  across the array in the form [6]

$$I_s = I_c \sin(\varphi/N). \quad (10)$$

The plasma frequency of junctions fabricated by Al– $\text{Al}_2\text{O}_3$ –Al technology reduces to the order of 20–100 Grad/s; moreover, it possesses much larger inductance and smaller  $\beta_c$ , which is usually referred to as a overdamped junction with large dissipation (small  $R_J$ ) and small capacitance [18]. These features are suitable for microwave superconducting electronics.

### III. DJTL

To construct a series-connected DJTL, a microstrip line is loaded in a periodic fashion by a series of unbiased JJ blocks, as sketched in Fig. 2.

This block can be a single junction,  $N$ -fold stacked JJs, array of trilayer junctions, or any other combination of junctions. The

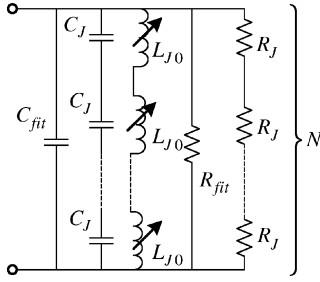


Fig. 3. JJ block with RCSJ model of each junction can be represented by a single effective junction.

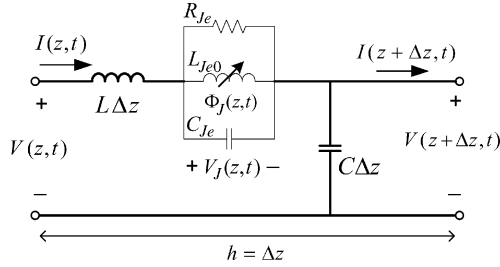


Fig. 4. Unit cell of periodically loaded series-connected DJTL.

proposed JJ block, which is used in our simulation part, as depicted in Fig. 3. It consists of an array of an identical unbiased junction in parallel to a fit capacitor  $C_{\text{fit}}$  and also fit shunt resistance  $R_{\text{fit}}$ . These extra fit elements are used to control the resistance, capacitance, and plasma frequency associated with the junction.

The critical currents, capacitances, normal-state junction resistances, and self-inductances are taken to be identical for all junctions. Moreover, like an array of JJ, this JJ block can be represented by a single effective junction. The TL model of this structure including its unit cell is illustrated in Fig. 4.

If the period of the structure ( $\Delta z$ ) is much less than the wavelength ( $\lambda$ ) of the microwave signal, i.e.,  $\Delta z \leq \lambda/20$ , we can exploit the long wave approximation ( $\Delta z/\lambda \rightarrow 0$ ) to form a set of differential equations to elucidate the nonlinear microwave propagation through this structure. Therefore, in a low-frequency limit, this structure can be described by a system of partial differential equations in the form of

$$\frac{\partial V}{\partial t} + \frac{1}{C} \frac{\partial I}{\partial z} = 0 \quad (11)$$

$$\frac{\partial I}{\partial t} + \frac{1}{L} \frac{\partial V}{\partial z} = \frac{-V_J}{L\Delta z} \quad (12)$$

$$\frac{\partial V_J}{\partial t} = \frac{1}{C_{Je}} I - \frac{1}{R_{Je} C_{Je}} V_J - \frac{I_c}{C_{Je}} \sin\left(2\pi \frac{\Phi_J}{\Phi_0}\right) \quad (13)$$

$$\frac{\partial \Phi_J}{\partial t} = V_J. \quad (14)$$

Note that  $R_{Je}$  and  $C_{Je}$  are lumped elements, but  $L$  and  $C$  are distributed elements. This is the reason of appearance  $\Delta z$  in (12).  $\Phi_J$  is also the flux associated to the nonlinear inductor (JJ),  $L_{Je0} = NL_{J0}$ ,  $C_{Je} = C_{\text{fit}} + C_J/N$ , and  $R_{Je} = NR_J R_{\text{fit}} / (NR_J + R_{\text{fit}})$ .

These equations are derived in a similar manner, which is usually used to form state equations in circuit theory. Supposing

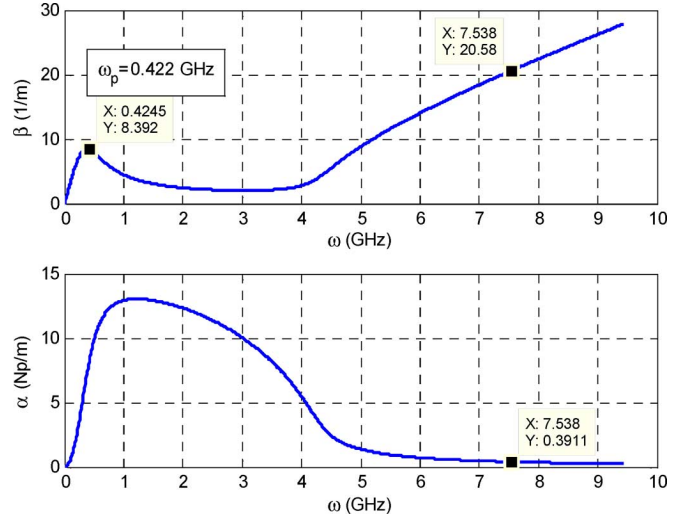


Fig. 5. Dispersion diagram of series-connected DJTL.  $L_{J0} = 0.17$  nH,  $C_J = 10$  fF,  $R_J = 50$   $\Omega$ ,  $N = 1000$ ,  $R_{\text{fit}} = 50$   $\Omega$ ,  $C_{\text{fit}} = 33$  pF,  $Z_0 = 50$   $\Omega$ ,  $L = 166$  nH/m,  $C = 66$  pF/m,  $h = 1$  cm.

that  $\Phi_J \ll \Phi_0$ , we can linearize the above equations by letting  $\sin(2\pi\Phi_J/\Phi_0) \sim 2\pi\Phi_J/\Phi_0$ . We then insert harmonic solutions given by  $Re\{A_i e^{j(\omega t - \gamma z)}\}$ ,  $i = 1, 2, 3, 4$  for all variables of  $V$ ,  $I$ ,  $V_J$ , and  $\Phi_J$  into (11)–(14). This procedure yields a homogeneous matrix equation in terms of complex coefficients of  $A_1$ ,  $A_2$ ,  $A_3$ , and  $A_4$ . The determinant of this matrix should vanish in order to have a nontrivial solution. Finally, it results in a dispersion relation between complex propagation constant  $\gamma = \beta - j\alpha$  and angular frequency  $\omega$  given by

$$\gamma^2 = \frac{LCL_{Je0}C_{Je}\omega^4 - C\left(L + \frac{L_{Je0}}{\Delta z}\right)\omega^2 - j\frac{LCL_{Je0}}{R_{Je}}\omega^3}{L_{Je0}C_{Je}\omega^2 - 1 - j\frac{L_{Je0}}{R_{Je}}\omega}. \quad (15)$$

Putting a voltage source  $V_s(t)$  with the associated series resistance  $R_S$  and a load impedance  $R_L$  at the ends of the DJTL and setting all variables to zero before  $t = 0$ , a set of complete well-posed equations including a system of partial differential equations (11)–(14) with mixed boundary conditions and zero initial values in the form of

$$V_s(t) = R_S I(0, t) + V(0, t) \quad (16)$$

$$V(z_{\text{max}}, t) = R_L I(z_{\text{max}}, t) \quad (17)$$

$$V(z, 0) = I(z, 0) = V_J(z, 0) = \Phi_J(z, 0) = 0. \quad (18)$$

By using an array of 1000 Al–Al<sub>2</sub>O<sub>3</sub>–Al junctions with parameters [18], [19]  $I_c = 2$   $\mu$ A,  $C_J = 10$  fF,  $R_J = 50$   $\Omega$ ,  $L_{J0} = 0.17$  nH, and fit elements of  $R_{\text{fit}} = 50$   $\Omega$  and  $C_{\text{fit}} = 33$  pF, the dispersion diagram is shown in Fig. 5. These Josephson blocks are mounted on a  $Z_0 = 50$   $\Omega$  microstrip line with distributed inductance  $L = 166$  nH/m and distributed capacitance  $C = 66$  pF/m at the equal-distance positions with a spatial period of  $h = 1$  cm. The wavelength at  $\omega = 9$  Grad/s is equal to 20 cm, so the period of  $\Delta z = 1$  cm is small enough to hold the slow-varying approximation, which has been assumed to derive the TL (11)–(14). With these parameters, the plasma frequency of the Josephson block is  $\omega_p = 0.422$  Grad/s, and the Stewart–

McCumber parameter of a single junction is  $\beta_c = 0.147$ , all suitable for microwave applications. As the JJ block is modeled by a resonant circuit, the resonance behavior is expected at plasma frequency. At the low-frequency domain, the inductive part of the JJ block behaves as a short circuit and at high frequencies the capacitive part of the block exhibits the same behavior. Therefore, in both regimes, the effect of the resistive part is reduced and we expect low attenuation. On the other hand, at the resonant frequency occurring at the plasma frequency, inductor and capacitor components of each block cancel each other, and the resistance part becomes more prominent by inducing large attenuation. Furthermore, according to Fig. 5, we observe nondispersive behavior below the plasma frequency (low frequency) and also far above it (high frequency). At low frequencies, the inductor elements are dominant components; however, at high frequencies, the capacitors of each block become dominant elements. Thus, slow wave propagation is expected at low frequencies in comparison to high frequencies. All the above expectations are observed clearly in the dispersion diagram of Fig. 5.

#### IV. FDTD METHOD

The first step in obtaining an FDTD solution is to set up a regular grid in space and time. Time and space steps are denoted by  $k$  and  $h$ , respectively, and the total number of temporal and spatial grids in the computational domain is referred by  $N$  and  $M$ . A few extra points beyond the computation domain might be added for numerical reasons. The next step is to approximate the differential equations with a proper finite-difference scheme. We used an explicit Lax–Wendroff scheme [20], [21], which is well suited for our problem. This scheme provides a second-order accuracy by itself so there is no need to complicate the implementation by defining additional grids points at half-time and half-space [22]–[24]. To apply the Lax–Wendroff scheme in our model, (11)–(14) are restated in the matrix form

$$\frac{\partial \mathbf{U}}{\partial t} = \mathbf{f}(\mathbf{U}) - \frac{\partial \mathbf{F}(\mathbf{U})}{\partial z} \quad (19)$$

where column vectors  $\mathbf{U}$ ,  $\mathbf{F}(\mathbf{U})$ , and  $\mathbf{f}(\mathbf{U})$  are defined as  $\mathbf{U} = [V \ I \ V_J \ \Phi_J]^T$ ,  $\mathbf{F}(\mathbf{U}) = [I/C \ V/L \ 0 \ 0]^T$  and

$$\mathbf{f}(\mathbf{U}) = \begin{bmatrix} 0 \\ \frac{-1}{L\Delta z} V_J \\ \frac{1}{C_{Je}} I - \frac{1}{R_{Je} C_{Je}} V_J - \frac{I_c}{C_{Je}} \sin\left(2\pi \frac{\Phi_J}{\Phi_0}\right) \\ V_J \end{bmatrix}. \quad (20)$$

Note that  $\mathbf{f}(\mathbf{U})$  is a nonlinear function of  $\mathbf{U}$ . Applying the Lax–Wendroff scheme, the update equation can be obtained as follows:

$$\begin{aligned} \mathbf{U}_m^{n+1} = & \mathbf{U}_m^n - \frac{\lambda}{2} [\mathbf{F}(\mathbf{U}_{m+1}^n) - \mathbf{F}(\mathbf{U}_{m-1}^n)] \\ & + \frac{\lambda^2}{2} \left\{ \mathbf{J}(\mathbf{U}_{m+\frac{1}{2}}^n) [\mathbf{F}(\mathbf{U}_{m+1}^n) - \mathbf{F}(\mathbf{U}_m^n)] \right. \\ & \quad \left. - \mathbf{J}(\mathbf{U}_{m-\frac{1}{2}}^n) [\mathbf{F}(\mathbf{U}_m^n) - \mathbf{F}(\mathbf{U}_{m-1}^n)] \right\} \\ & - k \frac{\lambda}{4} [\mathbf{J}(\mathbf{U}_{m+1}^n) \mathbf{f}_{m+1}^n - \mathbf{J}(\mathbf{U}_{m-1}^n) \mathbf{f}_{m-1}^n] \\ & + \frac{k}{2} (\mathbf{f}_m^{n+1} + \mathbf{f}_m^n) \end{aligned} \quad (21)$$

where  $\lambda = k/h$ ,  $\mathbf{U}_m^n$  is the value of matrix  $\mathbf{U}$  evaluated at  $z = mh$  and  $t = nk$  and  $\mathbf{J}(\mathbf{U}_m^n)$  is the 4-by-4 Jacobian matrix whose entries are defined by

$$\mathbf{J}_{i,j} = \frac{\partial \mathbf{F}_i}{\partial \mathbf{U}_j}, \quad i, j = 1, 2, 3, 4 \quad (22)$$

where  $\mathbf{F}_i$  and  $\mathbf{U}_j$  are the  $i$ th and  $j$ th element in column vectors  $\mathbf{F}$  and  $\mathbf{U}$ . To avoid midpoint evaluations, the Jacobian matrices can be found by

$$\mathbf{J}(\mathbf{U}_{m+\frac{1}{2}}^n) = \frac{\mathbf{J}(\mathbf{U}_m^n) + \mathbf{J}(\mathbf{U}_{m+1}^n)}{2} \quad (23)$$

$$\mathbf{J}(\mathbf{U}_{m-\frac{1}{2}}^n) = \frac{\mathbf{J}(\mathbf{U}_{m-1}^n) + \mathbf{J}(\mathbf{U}_m^n)}{2}. \quad (24)$$

Obviously, by applying an update equation of (21) into the ending points at the two boundaries, two fictitious points appear at each time step. Due to the possibility of generating instability, care should be taken to compute such points. Thus, we use the following relations to calculate extra-left and extra-right points, respectively, [20]:

$$\mathbf{U}_1^{n+1} = 2\mathbf{U}_2^{n+1} - \mathbf{U}_3^{n+1} \quad (25)$$

$$\mathbf{U}_{M+2}^{n+1} = 2\mathbf{U}_{M+1}^{n+1} - \mathbf{U}_M^{n+1}. \quad (26)$$

Based on (16) and (17), update equations for boundary conditions at the two ends of the TL are as follows:

$$I_2^{n+1} = \frac{V_s(t_{n+1}) - V_2^{n+1}}{R_s} \quad (27)$$

$$I_{M+1}^{n+1} = \frac{V_{M+1}^{n+1}}{R_L}. \quad (28)$$

It can be perceived that (21) involves four unknowns that are coupled to each other through four nonlinear equations so at each grid in the computational domain, a system of nonlinear simultaneous equations must be solved. A detailed procedure of the FDTD implementation is illustrated in the flowchart shown in Fig. 6.

#### V. NUMERICAL RESULTS

For many numerical simulations, when very small or very big numbers are involved, it is often helpful to normalize all parameters and variables to special values. The scaling rules for FDTD analysis of the DJTL is described in Table I. Basically, any scaling rule must have this important property such that when we substitute new normalized variables and parameters into the set of master equations for the problem, these equations hold the same form as they have for the nonnormalized variables and parameters. Hence, in order to establish a normalization rule in our problem, we choose four arbitrary constants, namely,  $\omega_0$ ,  $k_0$ ,  $Z_0$ , and  $I_0$ , to normalize frequency, wavenumber, impedance, and current by dividing them by these constants, respectively. All other remaining parameters and variables are then normalized into the proper form by using these four assumed parameters, as described in Table I. By putting new normalized variables into (11)–(14) or the dispersion relation of (15), this conclusion is drawn from the above discussion that  $\omega_0$ ,  $Z_0$ , and  $I_0$  can be taken as arbitrary constants, but  $k_0$  must be equals to  $1 \text{ m}^{-1}$ . A summary of the above process is shown in Table I.

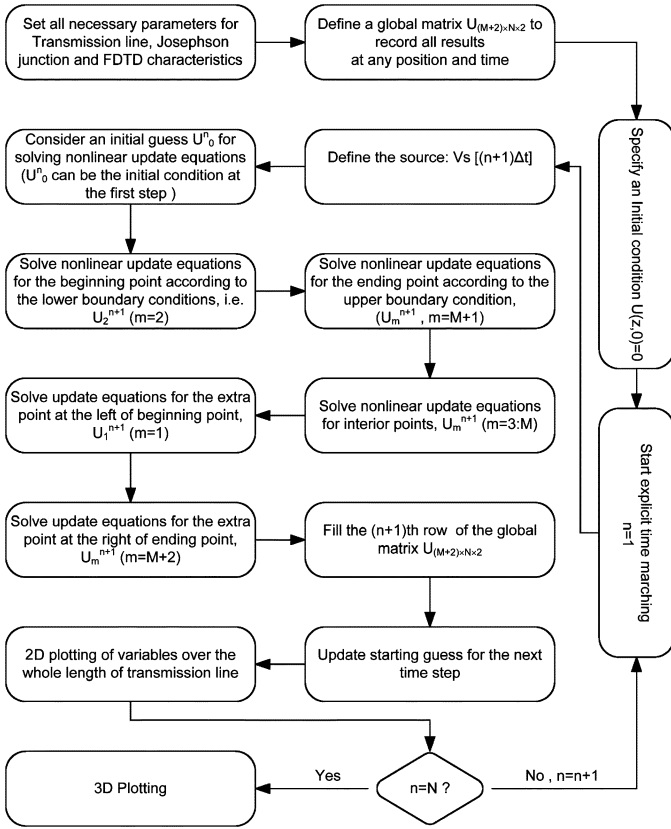


Fig. 6. Flowchart including all details for explicit implementation of FDTD to analyze the DJTL.

TABLE I  
NORMALIZATION RULE

Parameters and variables	Normalization rule
Frequency	$\tilde{\omega} = \omega/\omega_0$ , e.g. $\omega_0 = \omega_p$ or $\omega_0 = 3 \times 10^8$ Hz
Propagation constant	$\tilde{\gamma} = \gamma/k_0$ , $k_0 = 1m^{-1}$
Space	$\tilde{z} = zk_0$ , $k_0 = 1m^{-1}$
Time	$\tilde{t} = t\omega_0$
Impedance	$\tilde{R}_s = R_s/Z_0$ , $\tilde{R}_L = R_L/Z_0$ , $\tilde{R}_J = R_J/Z_0$ , e.g. $Z_0 = 50\Omega$
Inductance	$\tilde{L} = L\omega_0/Z_0$ , $\tilde{L}_{J0} = L_{J0}\omega_0/Z_0$
Capacitance	$\tilde{C} = C\omega_0Z_0$ , $\tilde{C}_J = C_J\omega_0Z_0$
Current	$\tilde{I} = I/I_0$ , i.e. $I_0 = I_c$
Voltage	$\tilde{V} = V/I_0Z_0$
Flux	$\tilde{\Phi} = \Phi\omega_0/Z_0I_0$

In order to conduct the FDTD simulation, we choose the same structure and also the same physical and geometrical parameters as described in Section III for calculating the dispersion diagram of Fig. 5. The normalization rule of Table I is applied into the actual parameters and variables of the problem by reference parameters  $Z_0 = 50 \Omega$ ,  $\omega_0 = 3 \times 10^8$  rad/s,  $I_0 = I_c = 2 \mu A$ , and  $k_0 = 1 m^{-1}$ . To be in a small amplitude regime, we drive the structure by a sinusoidal voltage source with amplitude of  $V_{smax} = 10 \mu V$  and frequency of  $\omega_s = 7.53$  Grad/s ( $f_s = 1.19$  GHz). The series resistance associated with the voltage source and also the load impedance at the end of the structure are  $R_s = R_L = Z_0 = 50 \Omega$ . After normalization, the new variables are given as  $\tilde{C}_J = 0.5$ ,  $\tilde{L}_{J0} = 1$ ,

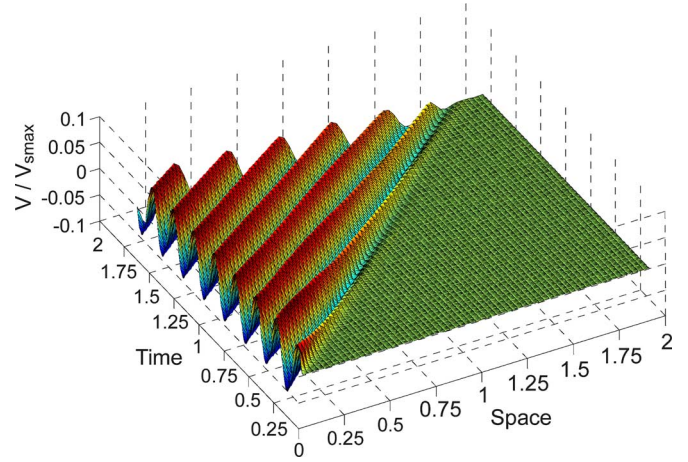


Fig. 7. Wave propagation in a DJTL analyzed by the RCSJ model,  $\tilde{L} = \tilde{C} = 1 m^{-1}$ ,  $\tilde{R}_J = \tilde{R}_L = \tilde{R}_s = 1$ ,  $\tilde{C}_J = 0.5$ ,  $\tilde{L}_{J0} = 1$ ,  $\tilde{f}_s = 4$ ,  $\tilde{V}_{smax} = 0.1$ ,  $\tilde{z}_{max} = 2$ ,  $\tilde{t}_{max} = 2$ ,  $h = 0.01$ ,  $k = 0.001$ .

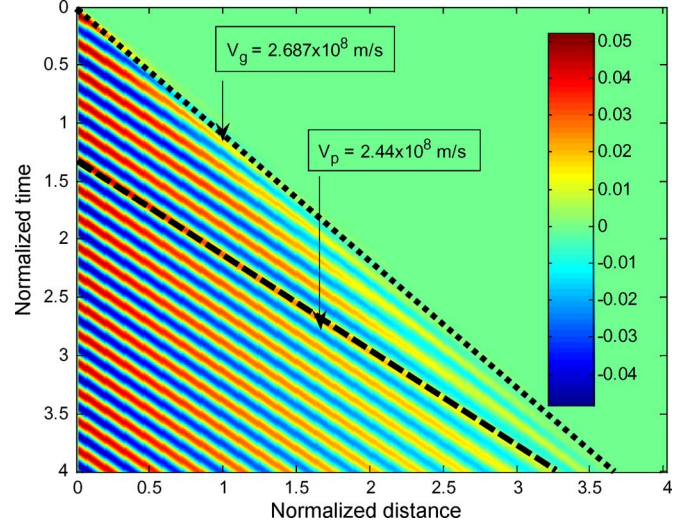


Fig. 8. Group and phase velocity for wave propagation in a DJTL based on the RCSJ model.

$\tilde{R}_J = \tilde{R}_L = \tilde{R}_s = 1$ ,  $\tilde{L} = \tilde{C} = 1 m^{-1}$ ,  $\tilde{f}_s = 4$ , and  $\tilde{V}_{smax} = 0.1$ .

Fig. 7 illustrates the voltage wave propagation in a series-connected DJTL over both space and time axes. Due to the abrupt jump from the resting initial condition to some values by the voltage source, many Fourier components (frequency components) are excited; hence, we observe dispersive behavior in the forefront of the wave as more clearly shown in Fig. 8, which is the top perspective of Fig. 7.

Due to the normal resistive channel  $R_J$ , the wave will attenuate gradually as sketched in the voltage profile of Fig. 9. However, the leading cycle of the wave train decays more compared to other cycles because of the dispersion effect that broadens it. By measuring the distance between two successive crests of the wave depicted in Fig. 9, the phase constant of the wave is found to be  $\beta = 20.9$  rad/m. Moreover, by simple algebraic calculation based on the data of Fig. 9, the attenuation constant is given as  $\alpha = 0.403$  Np/m. Both  $\alpha$  and  $\beta$  are in agreement with the result shown in dispersion diagram of Fig. 5. The magnitude of the

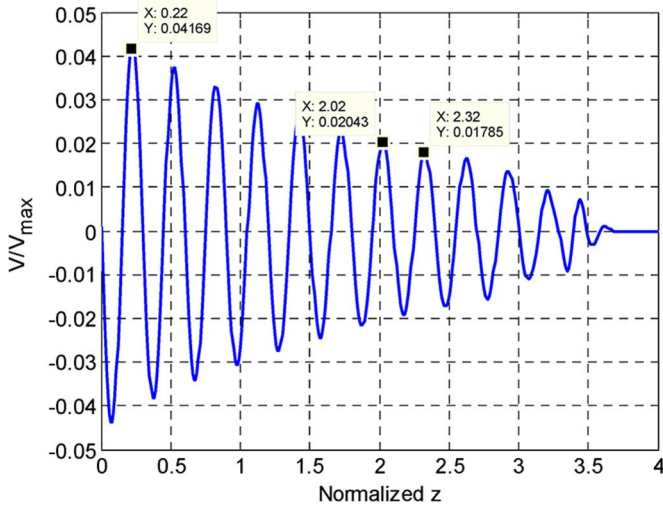


Fig. 9. Profile of the voltage pattern in series-connected DJTL. Attenuation and phase constant can be found from this figure.

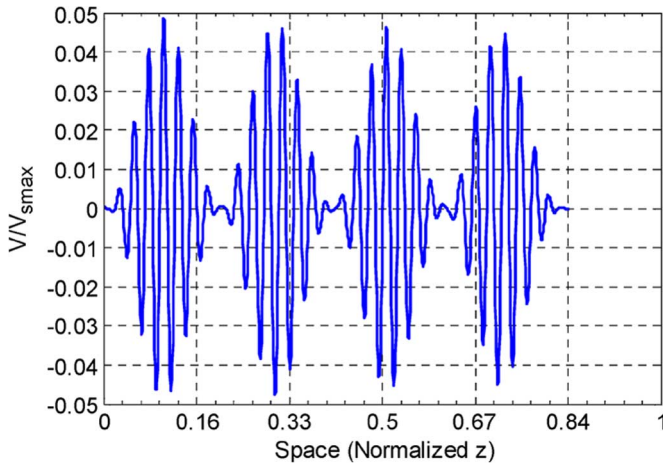


Fig. 10. Wave packet propagation in DJTL,  $\bar{f}_s = 32$ ,  $\bar{f}_n = 2$ .

voltage at the beginning of the line is half of the magnitude of the voltage source, as seen in Fig. 9, because of the impedance matching between the source and line.

The study of the wave packet introduces another interesting aspect of the DJTL. In the generalized RCSJ model of the JJ, the resistive element causes the dispersion behavior, which has already been seen in Figs. 7 and 8. This dispersive behavior can be monitored by the wave packet. The wave packet that we use is in the form of

$$V = V_{\text{smax}} \sin(\omega_s t) \sin^2(\omega_n t) \quad (29)$$

where  $\omega_s \gg \omega_n$ . The wave  $\sin^2(\omega_n t)$  is a relatively smooth function and plays the role of an envelope for the wave function  $\sin(\omega_s t)$ . The envelope travels at the group velocity and the crests of the wave function moves with phase velocity. As observed in Fig. 10, at different zero-crossing points of the envelope, the phase of the wave function changes, and this is evidence of dispersive behavior.

Numerical simulations reveal this important fact that, in some particular cases, the cutoff condition happens in the series DJTL.

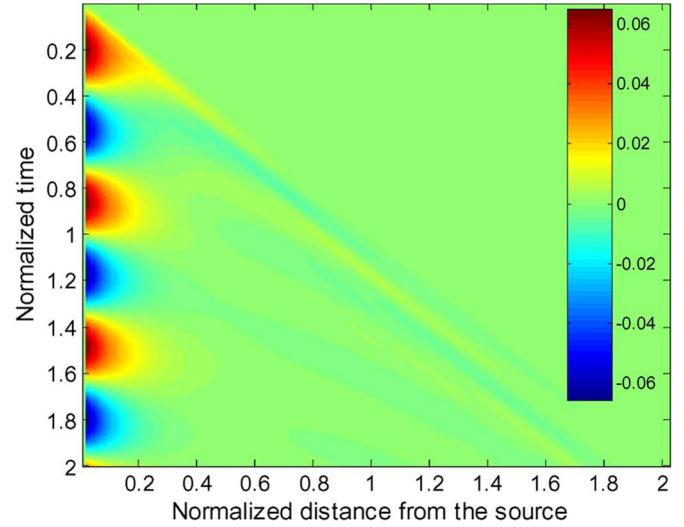


Fig. 11. When driving frequency is close enough to plasma frequency, DJTL reveals cutoff propagation.

One kind of cutoff condition happens when the DJTL is driven with frequencies very close to the plasma frequency. At these frequencies, resonance occurs in the series JJ blocks and the line becomes very lossy; therefore, the wave decays very fast. Fig. 11 shows the cutoff propagation when the frequency of the voltage source is  $\omega = 2.82$  Grad/s. This frequency is located in the interval of the dispersion curve (Fig. 5), where attenuation is large.

Spatial discreteness can cause another type of cutoff, which happens at the Bragg frequency. This observation is similar to the cutoff propagation in the parallel DJTL, which has been described by the discreteness factor [7], [25], [26]. This fact is fully explained in the Appendix. To simplify the problem, we replace all Josephson blocks with basic junctions by assuming that  $C_J \rightarrow 0$ ,  $R_J \rightarrow \infty$  and removing all fit elements  $C_{\text{fit}} \rightarrow 0$ ,  $R_{\text{fit}} \rightarrow \infty$ . In this case, the propagation condition is given by

$$f \leq \frac{1}{\pi h \sqrt{C(L + L_{J0}/h)}}. \quad (30)$$

For example, by setting  $\tilde{L} = \tilde{C} = 1 \text{ m}^{-1}$ ,  $\tilde{L}_{J0} = 0.2$ ,  $h = 0.02$  and sinusoidal source with frequency  $\bar{f}_s = 4$ , these parameters fail to satisfy (30) and instead of propagation we have a cutoff propagation in the steady-state solution of the analysis, as illustrated in Fig. 12 for  $\tilde{V}_s = 0.2$ . According to (30), at a given frequency, by increasing  $L$ ,  $C$ , or  $L_{J0}$ , the cutoff frequency decreases, so for large values of circuit parameters, we encounter blocking in wave propagation at lower frequencies. This fact has been reported for the parallel-connected DJTL [25], [26].

According to (4), nonlinear Josephson inductance increases with increasing current, so we expect that high-current sections of the waveform to propagate slower than the low-current sections. Qualitatively, as time evolves, the peak of a current (or voltage since both have the same profile) leaves behind the bottom. As a result, a wave with a steeping end can develop, which eventually leads to a jump discontinuity [27], as represented in Fig. 13. This type of wave, which takes the form of a

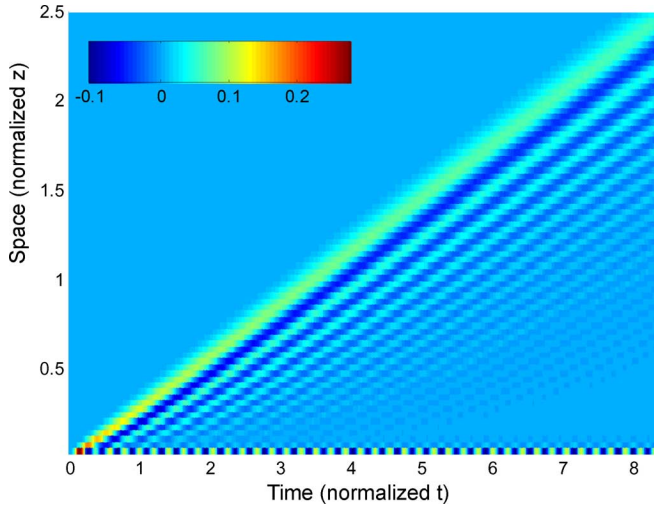


Fig. 12. Stopped-propagation of voltage wave through a DJTL,  $\bar{L} = \bar{C} = 1 \text{ m}^{-1}$ ,  $\bar{L}_{J0} = 10 \text{ m}^{-1}$ ,  $h = 0.02$ ,  $k = 0.002$ ,  $f_s = 4$ ,  $\bar{V}_s = 0.2$ .

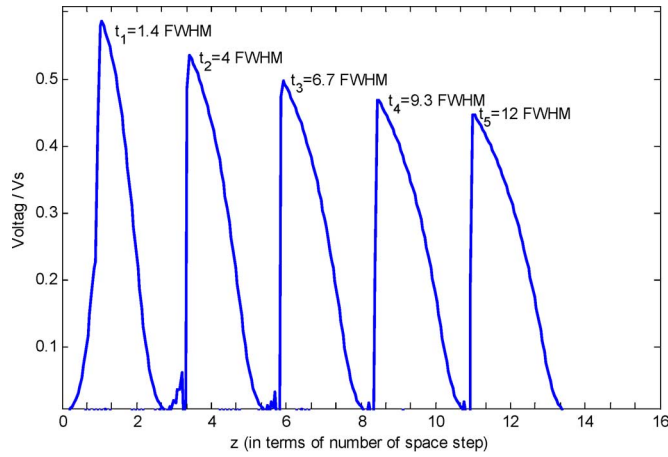


Fig. 13. Sketch of the formation of a shock wave in a nonlinear JJ transmission line,  $h = 2 \times 10^{-4}$ ,  $\text{FWHM} = 0.0053$ ,  $\bar{L} = \bar{C} = 1 \text{ m}^{-1}$ ,  $\bar{L}_{J0} = 1$ .

very sharp change, is called as a shock wave. To see this, the voltage source is chosen to be a Gaussian pulse in the form of

$$V_s(t) = V_{s\max} \exp \left[ -0.5 \left( \frac{t - t_d}{t_p} \right)^2 \right]. \quad (31)$$

The full wave half maximum (FWHM) of the Gaussian pulse has the relation

$$\text{FWHM} = 2\sqrt{2\ln(2)}t_p \cong 2.3548 t_p. \quad (32)$$

We choose  $t_p = k/0.125$  [28], where  $k = \Delta t$  is a normalized time step, which is  $2.82 \times 10^{-4}$ , and some other parameters are mentioned in Fig. 13. We have reduced the effect of the numerical dispersion, as displayed in Fig. 13, by having fine gridding and also running at a rate very close to the stability condition of Courant–Friedrichs–Lewy (CFL).

## VI. CONCLUSION

In this paper, a series-connected DJTL has been analyzed based on TL theory. Compared to the continuous Josephson TL,

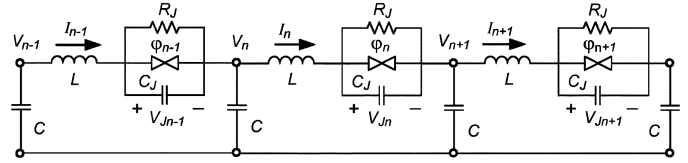


Fig. 14. Discrete circuit model of DJTL.

the DJTL has demonstrated more microwave compatibility because of its implementation on a regular TL. A discrete JJ block can be any combination of JJs and circuit elements, as pointed out in this paper. Moreover, a sample of a JJ block with its practical parameters was illustrated. Dispersion equations have been derived and different regimes based on the dispersion diagram and plasma frequency have been discussed. A rigorous, robust, and stable nonlinear FDTD based on the explicit Lax–Wendroff scheme has been developed to solve the nonlinear wave equations. Good agreement between the results of the dispersion diagram, which is based on the analytical treatment of the structure in the frequency domain and the results of the FDTD solver in time domain has been demonstrated. The cutoff propagation due to the resonance behavior of the Josephson block and also due to the discreteness of the structure has been described. Shock-wave formation has been observed when the DJTL was excited such that the flowing current is very close to the critical current of the junctions. This is an indication of the existence of a high nonlinear property in a typical DJTL with a potential application in realizing parametric devices such as traveling-wave amplifiers and mixers.

## APPENDIX

By dividing a series-connected DJTL into  $N$  identical unit cells, we can have another view of the DJTL, as illustrated in Fig. 14. Instead of continuous variable  $z$ , index  $n$  is designated for each unit cell.

Similar to the parallel-connected DJTL [7], we attain the following equation to express flux propagation in the structure:

$$\begin{aligned} & \frac{L_{J0}}{R_J} (\dot{\varphi}_{n-1} - 2\dot{\varphi}_n + \dot{\varphi}_{n+1}) \\ & + (\sin \varphi_{n-1} - 2\sin \varphi_n + \sin \varphi_{n+1}) \\ & + L_{J0}C_J (\ddot{\varphi}_{n-1} - 2\ddot{\varphi}_n + \ddot{\varphi}_{n+1}) \\ & = \frac{LCL_{J0}}{R_J} \varphi_n^{(3)} + LC \frac{d^2}{dt^2} [\sin \varphi_n] + LCL_{J0}C_J \varphi_n^{(4)} \\ & + CL_{J0}\ddot{\varphi}_n \end{aligned} \quad (33)$$

where  $\varphi_n$  is the flux associated to the JJ in the  $n$ th segment. In above equation, the first, second, third, and fourth derivatives of  $\varphi_n$  with respect to time are denoted by  $\dot{\varphi}_n$ ,  $\ddot{\varphi}_n$ ,  $\varphi_n^{(3)}$ , and  $\varphi_n^{(4)}$ , respectively. Considering a particular harmonic solution  $\varphi_n = A_0 e^{j(\omega t - \kappa n)}$  and small amplitude approximation ( $\sin \varphi_n \sim \varphi_n$ ), substituting this into (33), this yields the following dispersion relation:

$$4\sin^2(\kappa/2) = \frac{LCL_{J0}C_J\omega^4 - C(L + L_{J0})\omega^2 - j\frac{LCL_{J0}}{R_J}\omega^3}{L_{J0}C_J\omega^2 - 1 - j\frac{L_{J0}}{R_J}\omega}. \quad (34)$$

If  $L$  and  $C$  are distributed inductance and capacitance associated to the TL, they must be multiplied by the factor  $\Delta z$  before substitution in (33) and (34). Parameter  $\kappa$  in (34) is a complex number accounting for the attenuation and phase difference between two subsequent cells. If the phase constant and period of the uniform structure is  $\gamma$  and  $\Delta z$ , parameter  $\kappa$  will be equal to  $\gamma\Delta z$ . This equation is a modified version of (15) in a sense that the effect of the equi-spaced discrete Josephson element is taken into account. However, the uniform model of DJTL is a very good approximation in low-frequency regime. As frequency approaches the Bragg cutoff frequency,  $\sin^2(\kappa/2) = 1$ , the wave becomes dispersive, and these two dispersion relations deviate from each other.

If the long wave approximation ( $\Delta z/\lambda \rightarrow 0$ ) holds,  $\kappa$  is very small and by using  $2\sin^2(\kappa/2) \sim \kappa^2/2$ , two dispersion relations in (15) and (34) match very well. Note that when we are in a small amplitude approximation and temperature is low enough, most of the current consists of the Cooper pairs, so the normal and displacement currents are very small, thus,  $C_J \rightarrow 0$  and  $R_J \rightarrow \infty$ . By this assumption, the fluxon dynamics given by (33) and dispersion relation of (34) reduces to

$$(\sin \varphi_{n-1} - 2 \sin \varphi_n + \sin \varphi_{n+1}) = L_{J0} C \frac{d^2 \varphi_n}{dt^2} + LC \frac{d^2}{dt^2} [\sin \varphi_n] \quad (35)$$

$$\sin^2(\kappa/2) = \frac{1}{4} \omega^2 C(L + L_{J0}). \quad (36)$$

Therefore, to have a wave propagation condition, the following condition must be met:

$$\omega \leq \frac{2}{\Delta z \sqrt{C(L + L_{J0}/\Delta z)}} \quad (37)$$

as distributed elements  $L$  and  $C$  have been substituted by  $L\Delta z$  and  $C\Delta z$ , respectively. The right-hand side of this inequality is the Bragg cutoff frequency. The phase constant corresponding to the Bragg cutoff frequency is  $k = \pi\Delta z$  and this is in a quite good agreement with the fact that the first stopped band edge in periodic structures occurs at the half wavelength of the wave.

## REFERENCES

- [1] M. J. Lancaster, *Passive Microwave Device Applications of High-Temperature Superconductors*. Cambridge, U.K.: Cambridge Univ. Press, 1997.
- [2] R. R. Mansour, "Microwave superconductivity," *IEEE Trans. Microw. Theory Tech.*, vol. 50, no. 3, pp. 750–759, Mar. 2002.
- [3] G. W. Mitschang, "Space applications and implications of high temperature superconductivity," *IEEE Trans. Appl. Supercond.*, vol. 5, no. 2, pp. 69–73, Jun. 1995.
- [4] L. Frunzio, A. Wallraff, D. Schuster, J. Majer, and R. Schoelkopf, "Fabrication and characterization of superconducting circuit QED devices for quantum computation," *IEEE Trans. Appl. Supercond.*, vol. 15, no. 2, pp. 860–863, Jun. 2005.
- [5] M. R. Geller, E. J. Pritchett, A. T. Sornborger, and F. K. Wilhelm, "Quantum computing with superconductor Qbits," Cornell Univ., Ithaca, NY, Mar. 2006., arXiv:quant-ph/0603224 v1 24 [Online].
- [6] V. Kaplunenko and G. M. Fischer, "Josephson junction arrays as a variable inductor in RF circuits and tunable filters," *Supercond. Sci. Technol.*, vol. 17, pp. 145–149, Feb. 2004.
- [7] H. R. Mohebbi and A. H. Majedi, "Shock wave generation and cut off condition in nonlinear series connected discrete Josephson transmission line," *IEEE Trans. Appl. Supercond.*, vol. 19, no. 3, pp. 891–894, Jun. 2009.
- [8] A. V. Ustinov and M. Cirillo, "Fluxon dynamics in one-dimensional Josephson-junction arrays," *Phys. Rev. B, Condens. Matter*, vol. 47, no. 13, pp. 8357–8360, Apr. 1993.
- [9] P. Caputo, M. Darula, A. V. Ustinov, and H. Kohlstedt, "Fluxon dynamics in discrete Josephson transmission lines with stacked junctions," *J. Appl. Phys.*, vol. 1, no. 1, pp. 309–314, Jan. 1997.
- [10] H. S. J. van der Zant, D. Berman, and T. P. Orlando, "Fiske mode in one-dimensional parallel Josephson junction arrays," *Phys. Rev. B, Condens. Matter*, vol. 49, no. 18, pp. 12945–12952, May 1994.
- [11] C.-Y. E. Tong and R. Blundell, "Theory of series-connected distributed SIS mixers with ultra-wide instantaneous bandwidth," in *Proc. 17th Int. Space THz Tech. Symp.*, Paris, France, May 2006, pp. 35–38.
- [12] A. H. Majedi, S. K. Chaudhuri, and S. Safavi-Naeini, "Optical-microwave interaction modeling in high-temperature superconducting films," *IEEE Trans. Microw. Theory Tech.*, vol. 49, no. 10, pp. 1873–1881, Oct. 2001.
- [13] D. P. DiVincenzo, "The physical implementation of quantum computation," *Fortsch. Phys.*, vol. 48, no. 9, pp. 771–783, Oct. 2000.
- [14] A. Barone and G. Paterno, *Physics and Applications of the Josephson Effect*. New York: Wiley, 1982.
- [15] M. Tinkham, *Introduction to Superconductivity*. New York: McGraw-Hill, 1996.
- [16] D. Yohannes *et al.*, "Characterization of HYPRES' 4.5KA/CM2 & 8KA/CM2 Nb/ALOX/Nb fabricatiob process," *IEEE Trans. Appl. Supercond.*, vol. 15, no. 2, pp. 90–93, Jun. 2005.
- [17] "Niobium integrated circuit fabrication," Hypres, Elmsford, NY, Jan. 2008. [Online]. Available: <http://www.hypres.com/pages/download/designrules/DesignRules.pdf>
- [18] L. D. Jakcel, J. P. Gordon, E. L. Hu, R. E. Howard, and L. A. Fetter, "Decay of the zero-voltage state in a small area, high-current density Josephson junctions," *Phys. Rev. Lett.*, vol. 47, no. 9, pp. 697–700, Aug. 1981.
- [19] I. Siddiqi *et al.*, "Direct observation of dynamical bifurcation between two driven oscillation states of as Josephson junction," *Phys. Rev. Lett.*, vol. 94, pp. 1–4, Jan. 2005, 027005.
- [20] S. V. Lotkhov *et al.*, "Self-shunted Al/AlOx/Al Josephson junctions," Cornell Univ., Ithaca, NY, Feb. 2008, arXiv:cond-mat/0605532v1, arXiv.org [Online].
- [21] J. C. Strikwerda, *Finite Difference Schemes and Partial Differential Equations*. Philadelphia, PA: Soc. Ind. Appl. Math., 2004.
- [22] G. D. Smith, *Numerical Solution of Partial Differential Equations*. Oxford, U.K.: Clarendon, 1985.
- [23] A. Taflove and S. C. Hagness, *Computational Electrodynamics: The Finite-Difference Time-Domain Method*. Boston, MA: Artech House, 2005.
- [24] D. M. Sullivan, *Electromagnetic Simulation Using The FDTD Method*. Piscataway, NJ: IEEE Press, 2000.
- [25] G. D. Davidson, *Computational Electromagnetics for RF and Microwave Engineering*. Cambridge, U.K.: Cambridge Univ. Press, 2005.
- [26] A. M. Kadin, *Introduction to Superconducting Circuits*. New York: Wiley, 1999.
- [27] J. B. Keterson and S. N. Song, *Superconductivity*. Cambridge, U.K.: Cambridge Univ. Press, 1999.
- [28] G. J. Chen and M. R. Beasley, "Shock-wave generation and pulse sharpening on a series array Josephson junction transmission line," *IEEE Trans. Appl. Supercond.*, vol. 1, no. 3, pp. 140–144, Sep. 1991.
- [29] T. P. Montoya, "Improved 1-D FDTD modeling of parallel and series RLC loads in a lossless transmission line," in *IEEE AP-S Int. Symp.*, Albuquerque, NM, 2006, pp. 1583–1586.



**Hamid Reza Mohebbi** (S'09) was born in Tehran, Iran, on December 5, 1973. He received the B.Sc. degree in electrical engineering (with a major in telecommunication engineering) from the University of Tehran, Tehran, Iran, in 1996, the M.Sc. degree in electrical engineering (with a major in electromagnetic engineering) from Concordia University, Montreal, QC, Canada, in 2004, and is currently working toward the Ph.D. degree in electrical and computer engineering at the University of Waterloo, Waterloo, ON, Canada,

He is currently with the Department of Electrical and Computer Engineering and the Institute for Quantum Computing (IQC), University of Waterloo. His current activity is the investigation of novel parametric quantum microwave/millimeter-wave/terahertz devices based on nonlinear tunneling in superconductive JJs to be utilized in the read-out circuitry part of superconducting opto-electronic and quantum information processing devices. His research interests include microwave superconductivity, engineering quantum electrodynamics, and electromagnetic periodic structures.

Mr. Mohebbi was a recipient of the Ontario Graduate Scholarship (OGS).



the optical-microwave interaction in superconducting TLs for opto-electronic applications.

**A. Hamed Majedi** (S'00–M'02) was born in Tehran, Iran, on April 24, 1971. He received the B.Sc. degree in electrical engineering (with a major in microwave engineering) from the K. N. Toosi University of Technology, Tehran, Iran, in 1994, the M.Sc. degree in electrical engineering (with a major in photonics) from the Amir Kabir University of Technology, Tehran, Iran, in 1996, and the Ph.D. degree in electrical and computer engineering (with distinction) from the University of Waterloo, Waterloo, ON, Canada, in 2001. His doctoral dissertation concerned

After ten months as a Postdoctoral Fellow, he joined the Institute for Quantum Computing (IQC), University of Waterloo, as a Research Assistant Professor. He is currently an Assistant Professor with the Department of Electrical and Computer Engineering, University of Waterloo, cross-appointed to the Institute for Quantum Computing (IQC) and the Department of Physics, University of Waterloo, where he leads the Integrated Quantum Optoelectronics Laboratory (IQOL). His main research interests and activities include superconducting microwave/photonic devices, single photon detectors, terahertz opto-electronics, superconducting and photonic quantum devices for quantum information processing, plasmonics, and engineering quantum electrodynamics.